MIT Open Access Articles

Investigation of ion kinetic effects in direct-drive exploding-pusher implosions at the NIF

Massachusetts Institute of Technology

Investigation of Ion Kinetic Effects in Direct-Drive Exploding-Pusher Implosions at the NIF

M. J. Rosenberg,[a)] A. B. Zylstra, F. H. Séguin, H. G. Rinderknecht, J. A. Frenje, M. Gatu Johnson, H. Sio, C. J. Waugh, N. Sinenian, C. K. Li, and R. D. Petrasso

Plasma Science and Fusion Center, Massachusetts Institute of Technology, Cambridge, MA 02139, USA

P. W. McKenty, M. Hohenberger, P. B. Radha, J. A. Delettrez, V. Yu. Glebov, R. Betti, V. N.Goncharov, J. P. Knauer, and T. C. Sangster

Laboratory for Laser Energetics, University of Rochester, Rochester, NY 14623, USA

S. LePape, A. J. Mackinnon, J. Pino, J. M. McNaney, J. R. Rygg, P. A. Amendt, C. Bellei, L. R. Benedetti, L. Berzak Hopkins, R. M. Bionta, D. T. Casey, L. Divol, M. J. Edwards, S. Glenn, S. H. Glenzer, D. G. Hicks, J. R. Kimbrough, O. L. Landen, J. D. Lindl, T. Ma, A. MacPhee, N. B. Meezan, J. D. Moody, M. J. Moran, H.-S. Park, B. A. Remington, H. Robey, M. D. Rosen, S. C. Wilks, and R. A. Zacharias

Lawrence Livermore National Laboratory, Livermore, CA 94550, USA

H. W. Herrmann, N. M. Hoffman, G. A. Kyrala, R. J. Leeper, and R. E. Olson

Los Alamos National Laboratory, Los Alamos, NM 87545, USA

J. D. Kilkenny and A. Nikroo

General Atomics, San Diego, CA 92186, USA

(Dated: 9 December 2014)

Measurements of yield, ion temperature, areal density (ρR), shell convergence, and bang time have been obtained in shock-driven, D_2 and D^3He gas-filled "exploding-pusher" inertial confinement fusion (ICF) implosions at the National Ignition Facility (NIF) to assess the impact of ion kinetic effects. These measurements probed the shock convergence phase of ICF implosions, a critical stage in hot-spot ignition experiments. The data complement previous studies of kinetic effects in shock-driven implosions. Ion temperature and fuel ρR inferred from fusion-product spectroscopy are used to estimate the ion-ion mean free path in the gas. A trend of decreasing yields relative to the predictions of 2D DRACO hydrodynamics simulations with increasing Knudsen number (the ratio of ion-ion mean free path to minimum shell radius) suggests that ion kinetic effects are increasingly impacting the hot fuel region, in general agreement with previous results. The long mean free path conditions giving rise to ion kinetic effects in the gas are often prevalent during the shock phase of both exploding pushers and ablatively-driven implosions, including ignition-relevant implosions.

PACS numbers: 52.57.-z

I. INTRODUCTION

Thin, spherical glass shells were among the first capsules used in laser-driven inertial confinement fusion (ICF) research.[1–4] Known as "exploding pushers", these implosions are characterized by rapid heating of the thin shell, which explodes and drives a shock wave into the fuel. This shock wave compresses and heats the gas as it converges at the center of the capsule, and produces fusion reactions as it rebounds back through the fuel. This type of implosion is contrasted against implosions designed to achieve ignition and energy gain, which, in the final stage, are driven by the ablation of outer shell material and subsequent hydrodynamic compression of the fuel. These ablatively-driven implosions are currently under study at the National Ignition Facility (NIF) in the indirect-drive configuration.[5–10] Because shock-driven exploding-pusher implosions are mainly 1D

in nature and less sensitive to the complex hydrodynamic processes that characterize ablatively-driven implosions, such as hydrodynamic instabilities and mix, they are an ideal experiment to isolate and study the shock-convergence phase of ICF implosions.

For this reason, exploding pushers are an excellent platform to probe kinetic effects, which can be significant during the shock-convergence phase of ICF implosions, including ignition-relevant implosions.[11] Kinetic effects are often important in these moderate-density, high-temperature implosions where the mean free path for ion-ion collisions approaches the size of the burn region. Previous experimental work has investigated kinetic effects in shock-driven implosions and demonstrated the significance of ion diffusion and other long-mean-free-path effects that are not usually modeled in hydrodynamic codes.[12,13] In a systematic study of exploding pushers on OMEGA with a variety of initial gas densities, the ion-ion mean free path λ_{ii} and the Knudsen number $N_K \equiv \lambda_{ii}/R_{shell}$, the ratio of mean free path to minimum shell radius and a key figure of merit of ion kinetic effects, were varied from a regime that is

―――――――――
[a)] Electronic mail: mrosenbe@mit.edu

reasonably hydrodynamic-like ($N_K < 1$) to a regime that is strongly kinetic ($N_K \gg 1$).[12] The trend of increasing deviation from hydrodynamic models (such as the 1D radiation-hydrodynamics code DUED[14]) with increasing Knudsen number indicated the influence of ion kinetic effects. In agreement with this picture, another recent study by Le Pape *et al.* shows that in a high-density, low-temperature, short-mean-free-path, ($N_K \ll 1$) indirect-drive exploding pusher implosion, hydrodynamic codes are able to reproduce with high fidelity the experimental results.[15] In concert, these studies indicate that the ion-ion mean free path and the Knudsen number is a strong determinant of the applicability of hydrodynamic models.

To further investigate whether the trends observed in these prior experiments apply generally, under quite different experimental conditions (larger capsules, asymmetric illumination, oblate implosions), data were obtained on polar-direct-drive (PDD)[16] exploding pusher shots at the NIF that were conducted for diagnostic development and calibration.[17–19] In addition, given the scarcity of NIF shots for non-programmatic purposes, it is important to cull as much information and physics insight possible from these diagnostic development shots. These experiments produced copious DD and D^{3}He reactions, allowing for characterization of the implosions through measurement of two separate fusion yields, two different burn-averaged ion temperatures, fuel ρR in D$_2$ implosions and total ρR in both D$_2$ and D^{3}He implosions, x-ray images of the imploding shell and core, and x-ray and nuclear bang-times. This study employs 2D DRACO radiation-hydrodynamics simulations[20] for comparison to experimental data. As in prior work,[12] the experimentally-inferred ion-ion mean free path $\lambda_{ii} \propto T_i^2/n_i Z^4$ (where T_i is the ion temperature, n_i is the ion density, and Z is the ion charge), averaged over mean free paths calculated separately for different ion species in D^{3}He implosions,[21] is compared to the minimum shell radius R_{shell} to describe the degree of ion kinetic behavior. It is observed that the fusion yield relative to DRACO predictions varies inversely with the experimentally-determined N_K, suggesting that ion kinetic effects are beginning to degrade implosion performance. In Section IV, it is discussed that hydrodynamic mix does not account for these trends. As shown in Figure 1, it is evident that these results strongly match the findings of the previous experiments, which are presented together for guidance. The entire range of exploding pusher data shown in Figure 1 spans three orders of magnitude, between regimes of very low (10^{-2}) and very high (10) Knudsen numbers. While the OMEGA direct-drive experiments were conducted in a comprehensive, systematic way,[12] the experiments described in this work, conducted in a ride-along mode, produced a somewhat more complex set of data. However, in concert, these different experimental campaigns show how the discrepancy relative to hydrodynamic codes with increasing Knudsen number begins to be observed.
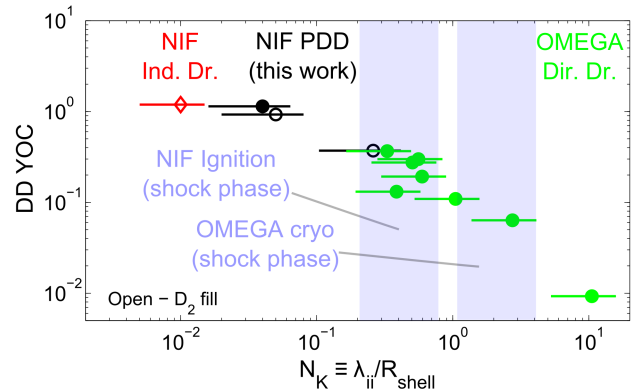

FIG. 1. (Color online) DD YOC as a function of the Knudsen number (N_K) for an indirect-drive exploding pusher on NIF (red diamond),[15] three polar-direct-drive (PDD) exploding pushers on NIF described in this work for which optimal DRACO simulations (including non-local electron transport and/or cross-beam energy transfer, see Section II) were performed, from left to right, shots N121128, N130129, and N120328 (black circles), and direct-drive exploding pushers on OMEGA (green circles).[12] Filled markers represent D^{3}He-filled implosions, while open markers denote D$_2$-filled implosions. Though the drive conditions are quite different, these experiments show a unified picture of the increasing impact of ion kinetic effects as a function of increasing Knudsen number above $N_K \gtrsim 0.1$. A band centered around $N_K = 0.5$ shows the approximate Knudsen number at the center of a NIF ignition-relevant indirect-drive or a NIF polar-direct-drive implosion immediately after shock convergence, while a band centered around $N_K = 2$ shows the approximate Knudsen number after shock convergence at the center of a cryogenic layered implosion on OMEGA.[22]

This paper is organized as follows: the experiments and models used for comparison to experimental data are described in Section II; experimental and some modeled results are shown in Section III; a discussion of the findings is presented in Section IV, with evidence of ion kinetic effects illustrated in Figure 8; and concluding remarks are presented in Section V.

II. EXPERIMENTS AND MODELING

Exploding-pusher implosions at the National Ignition Facility (NIF)[23] were conducted with ~192 laser beams pointed in the polar direct drive configuration,[16] delivering 40 to 130 kJ onto a capsule in a 1.4- or 2.0-ns ramp pulse. The experiments used 2.2 g/cm^3 SiO$_2$ shells with a 1530 to 1680-μm diameter and a thickness of 4.1 to 4.6 μm, filled with 10 to 12 atm. of D$_2$, D^{3}He, or HD^{3}He gas. Experimental parameters are summarized in Table I.

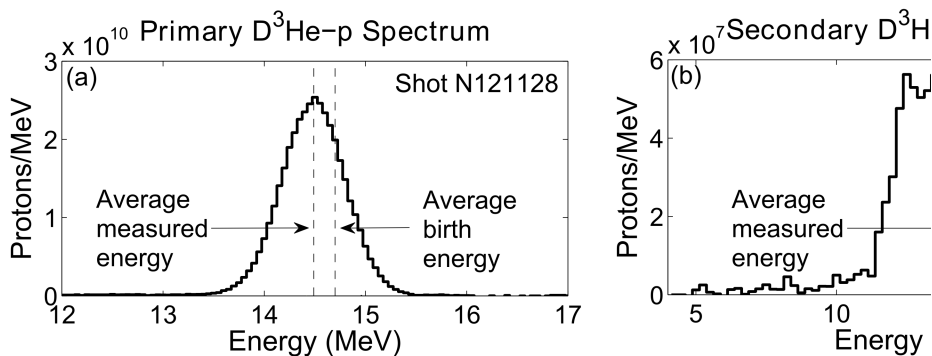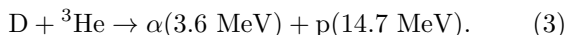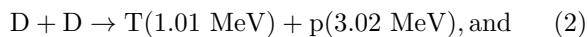The primary nuclear reactions used to diagnose the exploding-pusher implosions are:

$$\text{D} + \text{D} \rightarrow {}^3\text{He}(0.82 \text{ MeV}) + \text{n}(2.45 \text{ MeV}), \qquad (1)$$
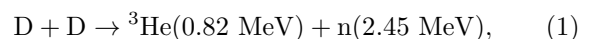
FIG. 2. (a) Measured primary D^3He-proton spectrum from D^3He exploding-pusher shot N121128 and (b) measured secondary D^3He-proton spectrum from D_2 exploding-pusher shot N110131. From the primary spectrum (a), the D^3He yield, D^3He-burn-averaged ion temperature (related to the spectral width as $T_i \propto \sigma^2$), and total ρR (proportional to energy downshift) are inferred. From the secondary spectrum (b), the total ρR is inferred from the energy downshift, while the ratio of secondary D^3He-proton to primary DD-neutron yield is proportional to the fuel ρR for $\rho R \leq 10$ mg/cm^2 (for $T_e \sim 5$ keV). Note the difference in energy-axis scale, as the secondary spectrum is much broader than the primary spectrum.

TABLE I. Capsule and laser parameters for exploding pushers used in this study, including: capsule outer diameter d; shell thickness Δr; total laser energy; approximate laser pulse duration; D_2 fill pressure; and ^{3}He fill pressure.

NIF Shot #	d (μm)	Δr (μm)	Energy (kJ)	Pulse (ps)	D_2 fill (atm.)	^{3}He fill (atm.)
N100823	1567	4.1	80.0	~2100	1.4	10.5[a]
N110131	1555	4.5	52.0	~2100	10.0	
N110722	1536	4.1	42.7	~1400	3.3	5.3
N120328	1555	4.4	130.6	~2100	9.9	
N121128	1682	4.3	43.4	~1400	3.3	5.8
N130129	1533	4.6	51.4	~1400	10.0	

[a] Capsule also contained 5.3 atm. H_2

$$D + D \rightarrow T(1.01 \text{ MeV}) + p(3.02 \text{ MeV}), \text{and} \quad (2)$$

$$D + {}^3He \rightarrow \alpha(3.6 \text{ MeV}) + p(14.7 \text{ MeV}). \quad (3)$$

In D_2 gas-filled implosions, ^{3}He fusion products (see equation 1) react with the thermal D fuel ions via the secondary reaction

$$^3He(\leq 0.82 \text{ MeV}) + D \rightarrow \alpha + p(12.6 - 17.5 \text{ MeV}). \quad (4)$$
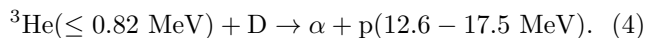
Sample primary and secondary D^3He-proton spectra are shown in Figure 2. From the primary spectrum, the D^3He yield, D^3He-burn-averaged ion temperature, and total ρR are inferred; from the secondary spectrum, the fuel ρR and total ρR are inferred. These and several other measurements are discussed in Section III.

For illustrative purposes, a 1D LILAC[24,25] simulation of mass-element trajectories and time-dependent temperature and fusion burn rates is shown in Figure 3 for a typical D^3He gas-filled exploding-pusher implosion at the

NIF (shot N110722). Fusion reactions are initiated primarily along the shock rebound trajectory (~1.8-2.0 ns), well before peak compression (~2.2 ns).
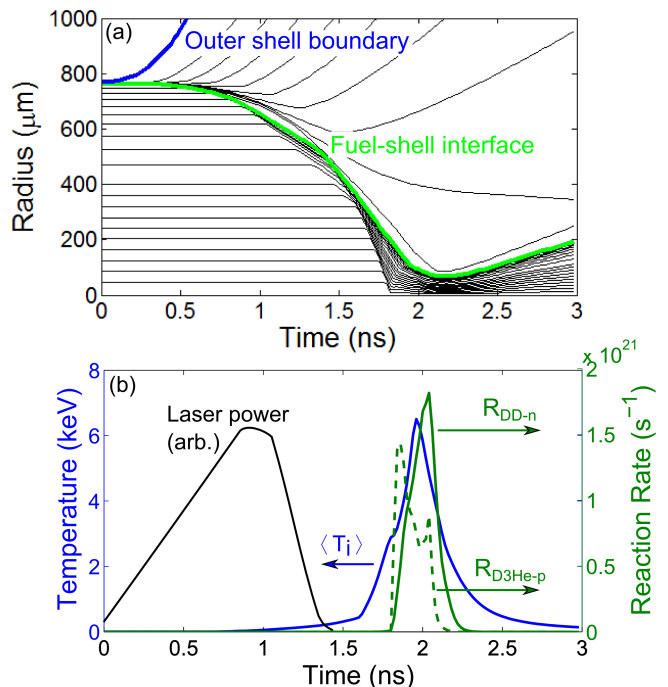
FIG. 3. (Color online) Illustrative 1D LILAC-simluated (a) Lagrangian mass element trajectories (black), (b) volume-averaged fuel ion temperature (blue), and rates of DD burn (green - solid) and D^3He burn (green - dashed) as a function of time in NIF D^3He exploding-pusher shot N110722 (4.1-μm-thick shell, 1536-μm diameter, 8.6 atm). A representative 1.4-ns-ramp laser pulse, approximately like that used in shot N110722, is also shown.

Primarily, the 2D hydrocode DRACO[20] was used to simulate these polar-direct-drive exploding-pusher experi-

ments at the NIF. DRACO simulations of ablatively-driven PDD experiments at the OMEGA laser facility[26] have been in good agreement with measured x-ray radiographs and ρR.[27,28] DRACO simulations have also been found to reasonably reproduce experimental yields, shell shape, and ρR in symmetrically-driven cryogenic implosions at OMEGA under conditions of high adiabat,[29–32] as in the present exploding pusher experiments. The use of 2D simulations is especially pertinent in these NIF exploding pusher experiments, where the polar direct drive (PDD) imposes an illumination asymmetry. 3D ray tracing is used to model inverse bremsstrahlung absorption of laser energy, and material equations of state were taken from SESAME tables. A flux-limited Spitzer thermal conductivity was used, with a flux limiter of 0.06.[33] To properly simulate the laser-absorption process and approximately capture the implosion velocity and shape in these exploding-pusher implosions, it is sometimes necessary to include models of non-local electron transport (NLET)[34] and cross-beam energy transfer (CBET).[35] Including CBET has been found to be necessary to reasonably reproduce implosion shape for higher laser intensities (laser energy >100 kJ for these NIF exploding pushers). Observables such as yield, ion temperature, ρR, bang time, and shell convergence and symmetry are calculated both from the more computationally intensive DRACO simulations that include NLET and/or CBET (performed for three of the experiments in this study) as well as from "nominal" DRACO simulations (performed for all of the experiments in this study), which do not include these models.

III. RESULTS

In the following sections, the measured fusion yields, burn-averaged ion temperatures, fuel and shell ρR, bang times, shell convergence, and shape are presented and, where appropriate, compared to DRACO-simulated values. Experimental measurements are summarized in Table II. It will be shown later that deviations from DRACO yield predictions are suggestive of ion kinetic effects.

A. Yield

DD-neutron yields were measured using the neutron time-of-flight (nTOF)[36,37] diagnostic suite and DD-proton yields were measured with an accuracy of about ±10% using the solid-state nuclear track detector CR-39.[19,38,39] The D^3He-proton yields and spectra were measured using wedge-range-filter (WRF) proton spectrometers[38,40,41] (a sample spectrum is shown in Figure 2). The measured D^3He yields shown in Figure 4b are averages of several measurements. The overall uncertainty in the yield measurements on a given shot is ~±10%.[42]
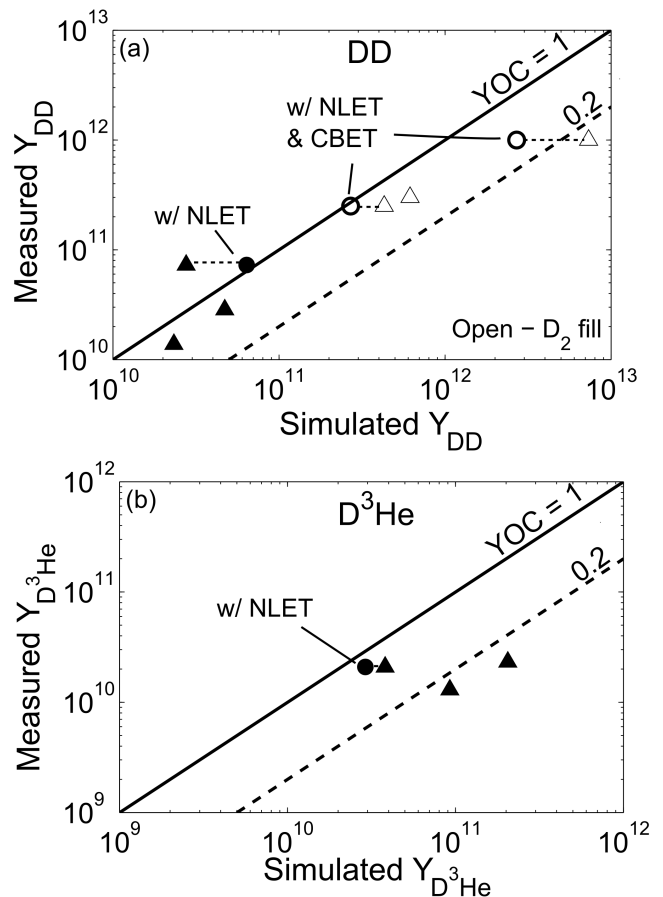

FIG. 4. (a) Measured DD-neutron yield and (b) D^3He-proton yield as a function of DRACO-simulated yields. The triangles represent the comparison of data to nominal DRACO simulations, while the circles represent the comparison of data to DRACO simulations that have included non-local electron transport (NLET) and cross-beam energy transfer (CBET). When both nominal and NLET/CBET DRACO simulations have been performed for a given experiment, those points are connected by a dotted horizontal line. Open markers denote D_2-gas-filled implosions, while filled markers denote D^3He-gas-filled implosions; the D^3He-filled shots in (b) are the same as those shown in (a). Yield-over-clean (YOC) values of 1 (solid line) and 0.2 (dashed line) are indicated. The measured yields are averaged over several measurements on each shot, with an overall error of ~±10%, approximately the size of the symbols.

A comparison of measured and nominal DRACO-simulated DD yields from D_2- and D^3He-gas-filled exploding pushers (Figure 4a) reveals that experimental values cluster around a yield-over-clean (YOC) – the ratio of measured yield to yield simulated by a "clean" hydrodynamic simulation that does not include a turbulent mix model or kinetic effects – of ~0.5-0.6. The NLET-CBET DRACO simulations have a YOC closer to 1. The experimental and nominal DRACO-simulated data show that the D^3He yield is, on average, 0.27 of the nomi-

TABLE II. Measured observables from these exploding pushers, including: DD yield; D³He yield; DD-burn-averaged ion temperature; D³He-burn-averaged ion temperature; bang time (x: x-ray, p: D³He-proton, n: DD-neutron); fuel ρR; and total ρR.

NIF Shot #	Y_{DD}	Y_{D^3He}	T_{iDD} (keV)	T_{iD^3He} (keV)	Bang Time (ps)	Fuel ρR (mg/cm²)	Total ρR (mg/cm²)
N100823	1.38×10^{10}	2.32×10^{10}	10.5	16.2			13
N110131	3.01×10^{11}		5.4		2430 (x)	4.6	23
N110722	2.85×10^{10}	1.30×10^{10}	8.8	15.1	1910 (x)		11
N120328	1.00×10^{12}		11.4		1770 (x)	3.6	
N121128	7.27×10^{10}	2.09×10^{10}	7.1	11.0	1880 (p)		9
N130129	2.50×10^{11}		4.0		2470 (n)	4.6	18

nal 2D DRACO simulated value (with a standard deviation of 0.20). Overall, the observed implosion performance relative to simulations is slightly worse for pure D_2 and higher-yield (higher-T_i) implosions, such as shot N120328, which is indicative of ion kinetic effects reducing the yield relative to hydrodynamics simulations in implosions with longer ion mean free paths.

B. Ion Temperature

To explore trends within the yield data to elucidate the possible role of ion kinetic effects, the yield results are presented together with measured burn-averaged ion temperatures. The DD-burn-averaged ion-temperature was measured by nTOFs and the D³He-burn-averaged ion temperature was determined from the Doppler width of the measured D³He proton spectrum (see Figure 2a), as measured by WRFs.[38,43,44] In NIF exploding-pusher implosions, the measured D³He-proton linewidth is dominated by thermal broadening.[45] Other capsule-related broadening effects (e.g. ρR evolution and implosion geometry) account for a broadening of $\sigma \sim 100$ keV in NIF exploding pusher implosions,[46] and are subtracted in quadrature from the measured linewidth. Additional broadening effects that are difficult to quantify on a shot-by-shot basis are not accounted for in this analysis, and thus set an upper limit on the linewidth-inferred ion temperature. Random turbulent flows are a potential spectral broadening mechanism,[47] which may cause the inferred ion temperature to slightly exceed the actual value across the data set.[48] Radial flows, more likely to be present in these shock-driven implosions than random, turbulent flows, would cause additional spectral broadening as well as a flattening of the spectral shape;[49] however, such distortion is not observed in the fusion product spectra (see Figure 2a). For the purposes of this analysis, in which only the trends of yield with ion temperature from one experiment to the next are paramount, the Doppler broadening of the fusion product spectra is used as a reasonable measure of the burn-averaged ion temperatures. Uncertainties in the different measurements are ~ 0.5 keV for the nTOF DD-burn-averaged temperature
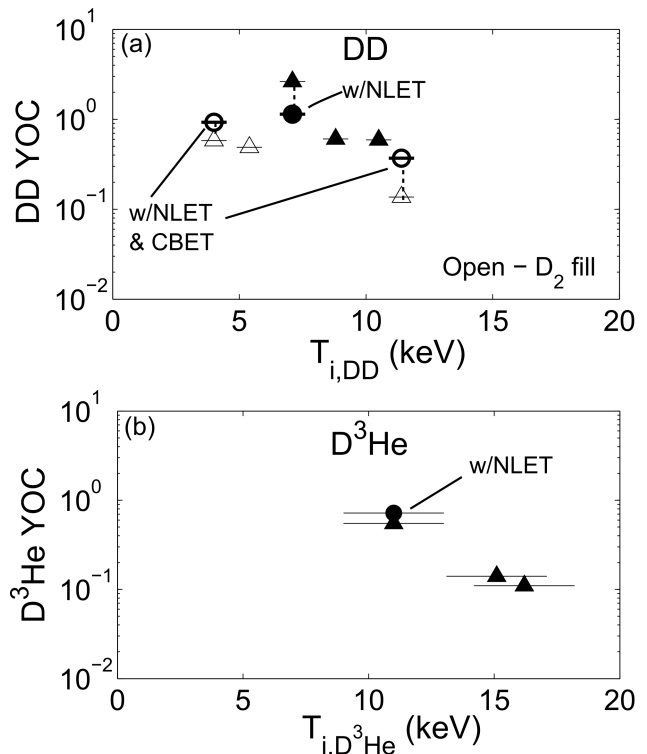
and ~ 2 keV for the D³He-burn-averaged temperature.

FIG. 5. (a) DD YOC as a function of the measured DD-burn-averaged ion temperature ($T_{i,DD}$) and (b) D³He YOC as a function of the measured D³He-burn-averaged ion temperature ($T_{i,D3He}$). The triangles represent the comparison of data to nominal DRACO simulations, while the circles represent the comparison of data to DRACO simulations that have included non-local electron transport (NLET) and cross-beam energy transfer (CBET). When both nominal and NLET/CBET DRACO simulations have been performed for a given experiment, those points are connected by a dotted vertical line.

The measured DD and D³He burn-averaged temperatures are compared to the DRACO YOCs in Figure 5. Over the set of experiments, the ion temperature varies as a consequence of variation in laser power, as the im-

plosion with the greatest laser power, shot N120328, has the highest DD-burn-averaged ion temperature. Both sets of data show a trend of decreasing YOC with increasing burn-averaged T_i over the range of 4 to 15 keV, with a more apparent trend among the D^{3}He data. This trend indicates that ion kinetic effects may be reducing the yield relative to hydrodynamics simulations in implosions with higher temperatures and, thus, longer ion mean free paths. Though accounting for the effect of bulk flows on fusion product spectral widths may cause a reduction in the inferred ion temperatures overall, it would not significantly alter this trend.

In general, nominal DRACO-simulated ion temperatures are in reasonable agreement with experimental measurements. This is especially the case for the D$_2$-filled shots, where measured and nominal DRACO-simulated DD-burn-averaged ion temperatures differ by no more than 15% over a large range in ion temperature and in YOC. Thus, these results demonstrate that the trend of decreasing YOC with increasing T_i is not merely a consequence of a hydrodynamics-related temperature discrepancy.

As an aside, the measured difference between DD-burn-averaged and D^{3}He-burn-averaged ion temperatures (x-axis values shown in Figures 5a and 5b) is not a sign of diagnostic disagreement, but rather is symptomatic of profiles and temporal evolution of density and temperature throughout the burn. Relative to the DD fusion reactivity, the D^{3}He reactivity has a stronger temperature dependence and is weighted more strongly by the hotter regions of the implosion. Ion temperature gradients therefore produce measurable differences in the burn-averaged ion temperatures of different reactions, as have been observed in the experimental data as well as in average-ion hydrodynamic codes, such as LILAC and DRACO, that do not allow for distinct ion temperatures for D and ^{3}He ions. Though in principle shock-heated D and ^{3}He ions can attain different temperatures in D^{3}He-filled implosions,[50] in these particular experiments, thermal decoupling of the different ions in the D^{3}He experiments is unlikely to be significant. For typical plasma conditions in the D^{3}He-filled implosions, with $n_i \sim 7 \times 10^{22}$ cm^{-3} and $T_i \sim 10$ keV, the thermal equilibration time between D and ^{3}He ions is only 25 ps, significantly shorter than the duration of the fusion reactions (likely 100-200 ps). Thus, the ions in the D^{3}He-filled implosions would quickly equilibrate to each other.

C. ρR and Convergence

Measurements of fuel ρR, total ρR, and shell convergence provide information about the fuel assembly in these low-convergence, shock-driven implosions, and can be used to help identify the approximate ion density n_i, ion mean free path λ_{ii}, and minimum shell radius R_{shell}. The ratio of these lengths, $N_K \equiv \lambda_{ii}/R_{shell}$, is a figure-of-merit that will be used in the assessment of ion kinetic effects, as discussed further in Section IV.

In D$_2$ implosions, for fuel ρR below $\sim$10 mg/cm^2, the fuel ρR is proportional to the ratio of secondary D^{3}He-p to primary DD-n yields.[51–53] For shot N110131, a secondary-proton yield of $2.0\pm0.5\times10^8$ (see Figure 2b) and a primary DD-neutron yield of $3.0\pm0.3\times10^{11}$ gives a fuel ρR of 4.6 ± 1.1 mg/cm^2, using a model of uniform fusion production throughout the fuel.[52] Similar measurements give a fuel ρR of 3.6 ± 1.1 mg/cm^2 for shot N120328 and 4.6 ± 1.1 mg/cm^2 for shot N130129. The fuel ρR does not significantly change from one implosion to the next, suggesting that differences in implosion performance relative to DRACO are unlikely to be caused by differences in hydrodynamic processes between the different implosions. These fuel ρR measurements are used to estimate the implosion convergence ratio, as $C = (\rho R_f/\rho R_{f0})^{1/2}$, where ρR_{f0} is the initial fuel areal density. With $\rho R_{f0} \sim 0.13$ mg/cm^2 for these three D$_2$-filled implosions, convergence ratios of $\sim$5.3-6.0 are inferred.

Total ρR data is not directly used to evaluate hydrodynamic-kinetic parameters, but is presented for completeness and as a consistency check on the approximate convergence ratios inferred from the fuel ρR measurements. The total ρR is inferred from the energy downshift of the secondary or primary D^{3}He-proton spectrum, as shown in Figure 2.[41] Assuming an average secondary-proton birth energy of 14.96 MeV[54] and measured energies of 14.08 ±0.15 MeV on the equator and an average energy of 14.33±0.15 MeV on the pole, total ρR of $\sim$26$\pm$5 and $\sim$19$\pm$5 mg/cm^2, respectively, are inferred for shot N110131 (Figure 2b). An average total ρR of 18$\pm$5 mg/cm^2 is inferred on D$_2$ shot N130129, while no total ρR measurement is possible for shot N120328 as the spectrum is net upshifted relative to the birth energy, an effect which is present only for that shot.[55] For D^{3}He-filled implosions, the birth energy of the primary D^{3}He-p spectrum is taken to be 14.7 MeV. D^{3}He shot N121128 (see Figure 2a) was measured to have a total ρR of 9$\pm$4 mg/cm^2, while a total ρR of 13$\pm$4 mg/cm^2 was obtained on shot N100823 and 11$\pm$4 mg/cm^2 was measured on shot N110722. These total ρR values, generally 10-20 mg/cm^2, are a factor of 10-20 greater than the initial ρR in the shell of $\sim$1 mg/cm^2. The shell ρR data are roughly consistent with the convergence ratio of $\sim$6 that was inferred from the fuel ρR, when allowing for some blowoff of outer shell material.[56]

X-ray emission gives a sense of the core size around bang time and may be used to estimate the implosion convergence and the length scale of the fuel, which can be compared to λ_{ii} to evaluate the likely impact of ion kinetic effects. Gated x-ray imaging diagnostics, the hardened gated x-ray imager (hGXI)[57] and the gated x-ray detector (GXD),[58] were used to capture images of the implosions. Figure 6 shows a measured x-ray emission image from the imploded core as captured by hGXI on shot N121128, $\sim$100 ps before bang time (no image at bang time was obtained). The image shows a core ra-
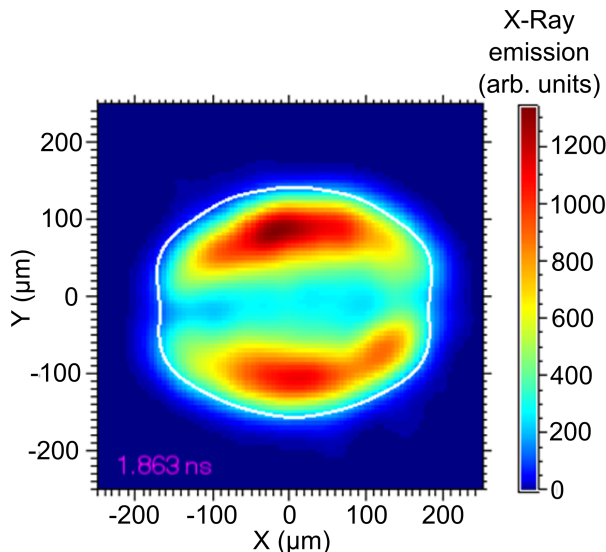
FIG. 6. (Color online) hGXI x-ray self-emission of the imploded core ~100 ps before bang time in D^{3}He exploding-pusher shot N121128. The image, with 10% peak emission contour (white line) indicated, shows an average P0 =168 μm and a P2/P0 = -0.13 (13% oblate). The P0 at bang time is extrapolated to be ~150 μm. The measured radius R_{shell} is used as a scale length of the implosion in calculation of the Knudsen number $N_K \equiv \lambda_{ii}/R_{shell}$.

inferred from the fuel ρR and total ρR.[59]

TABLE III. Measured fuel ρR, total ρR, x-ray emission radius P0 (contour of 10% of maximum brightness for N121128, 17% of maximum brightness for the others; the choice of contour imposes only a 5% uncertainty), and relative magnitude of second Legendre mode (P2/P0), the dominant asymmetry in the implosion. This ratio quantifies the deviation in core shape from spherical symmetry, with a negative value signifying an oblate implosion. These measuremets are used to quantify the ion-ion mean free path and implosion size, to assess the likely impact of ion kinetic effects.

Shot	Fuel ρR (mg/cm^2)	Total ρR (mg/cm^2)	X-Ray P0 (μm)	P2/P0
N100823		13±4		
N110131	4.6±1.1	23±5	89	-0.24
N110722		11±4	115	-0.33
N120328	3.6±1.0		182	-0.10
N121128		9±4	150	-0.13
N130129	4.6±1.1	18±5	94	-0.09

dius, expressed as the Legendre mode P0 of ~168 μm and an oblateness, characterized by a Legendre P2/P0, of ~-0.13. The shell is still converging at this time, and the core size at bang time is extrapolated to be ~10% smaller than inferred from this image. The estimated shell radius at bang time for N121128 is therefore taken to be 150 μm, and this extrapolation has only a small impact on the calculation of N_K shown later. The oblateness, present across this set of implosions as a consequence of the polar drive (with the x-ray P2/P0 ranging from -0.09 to -0.33 oblate, and also evident in the total ρR asymmetry observed on shot N110131), shows significant differences from previous, symmetrically-driven implosions on OMEGA,[12] which did not measurably deviate from spherical symmetry. This oblateness also demonstrates the importance of using a 2D code such as DRACO for comparison to experimental results. DRACO simulations that include NLET reasonably capture the implosion shape for shot N121128.

A summary of the measured fuel ρR, total ρR, implosion size, and symmetry is presented in Table III. The implosion radius around bang time (P0) varies as a consequence of the different laser pulses. Longer laser pulses, such as on shot N110131, drive the converging shell for a longer period and can produce a smaller implosion. Higher laser intensities, such as on shot N120328, produce a more rapid shock convergence, so that bang time occurs when the shell is at a somewhat larger radius. The P0 values across this set of exploding pushers imply convergence ratios of ~4-8, roughly in agreement with those

D. Bang Time

In order to assess the possible role of ion kinetic effects, it is important to determine that yield trends relative to DRACO are not the result of discrepancies in the energy coupling to the implosion. The energy coupling and, consequently, the implosion velocity, is assessed by measurements of nuclear and x-ray bang times – the times of peak fusion and x-ray production in the core. Bang time measurements using D^{3}He-protons and DD-neutrons were made by the particle time of flight (pTOF) diagnostic.[60] X-ray bang times were measured using the south pole bang time (SPBT) diagnostic[61] and gated x-ray imaging diagnostics, hGXI[57] and GXD.[58] These measured bang times are summarized and compared to DRACO-simulated DD-neutron bang times in Table IV. Uncertainty in the pTOF-measured DD-neutron bang time is ~±120 ps, while the uncertainty in the D^{3}He-proton bang time measurements is ~±100 ps. Uncertainty in the x-ray bang time is ~±100 ps. pTOF traces used to infer nuclear bang times on shots N121128 and N130129 are shown in Figure 7. Comparing the nuclear bang times, the measured D^{3}He bang time on shot N121128, 1880±100 ps, is in reasonable agreement with the DRACO DD bang time of 2020 ps, while the measured DD bang time on shot N130129, 2470±120 ps, is in good agreement with the DRACO DD bang time of 2530 ps. The overall trend indicates that DRACO captures the basic implosion dynamics and energy coupling to these shock-driven implosions fairly well.
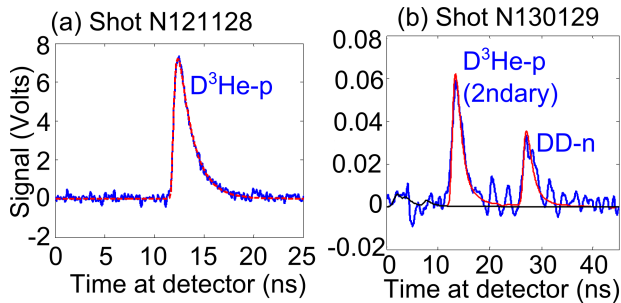
FIG. 7. (Color online) pTOF signal obtained on (a) D^3He shot N121128 and (b) D_2 shot N130129, used to infer nuclear bang times.

TABLE IV. Measured nuclear and x-ray bang times and DRACO-simulated DD-n bang times. The nuclear measurements were made using D^3He protons (p) on N121128 and with DD neutrons (n) on N130129.

Shot	Measured Bang Times		DRACO Bang Time
	Nuclear	X-Ray	Nuclear (DD-n)
	(ps)	(ps)	(ps)
N110131		2430	2650
N110722		1910	2150
N120328		1770	1990
N121128	1880 (p)	2000	2020
N130129	2470 (n)		2530

IV. DISCUSSION

While DRACO simulations model the overall implosion dynamics and energy coupling in these shock-driven implosions fairly accurately, trends within the nuclear yield data point to ion kinetic effects impacting fusion production. To estimate the significance of ion kinetic effects, the ion-ion mean free path around bang time, λ_{ii}, which varies in these implosions on the basis of the fuel composition (Z), T_i, and n_i, is evaluated. The ion temperature in the fuel around bang time is calculated to be the DD-burn-averaged T_i in D_2 implosions and the yield-weighted average of the DD- and D^3He-burn-averaged ion temperature in D^3He implosions. The ion density is estimated from the measured fuel ρR as $n_i = n_{i0}(\rho R_f/\rho R_{f0})^{3/2}$, assuming mass conservation and spherical symmetry, where n_{i0} and ρR_{f0} are the initial gas ion density and the initial fuel ρR, respectively. This calculation is performed directly for D_2 shots on which fuel ρR data was obtained, and a similar implied convergence ratio (~ 6) is also assumed for the D^3He shots. The fuel ρR and, therefore, the ion density, does not change significantly between the different implosions. These experimental quantities are used to estimate λ_{ii} around bang time, which is compared to the minimum shell radius R_{shell} as given by the x-ray P0.

As shown in Figure 8, the Knudsen number $N_K \equiv$

λ_{ii}/R_{shell} varies by a factor of ~ 7 over these exploding-pusher implosions, largely as a consequence of different fuel ion Z and ion temperature. For $N_K \ll 1$, the implosion behaves more hydrodynamically, whereas for $N_K \gtrsim 0.3$, kinetic effects start to become significant.[12] The moderate-temperature, D^3He-filled shot N121128 is the most hydrodynamic-like implosion, where $T_i = 8.0$ keV, $n_i \sim 7 \times 10^{22}$ cm^{-3}, and $Z = 1.47$ (a small, known amount of ^3He leaks out of the capsule before it is shot, reducing Z to slightly below 1.5), resulting in a λ_{ii}, after averaging over distinct mean free paths for D and ^3He ions, of ~ 6 μm.[62] Under these conditions, and with $R_{shell} = 150$ μm, N_K is ~ 0.04 for N121128. In contrast, the high-temperature, D_2-filled shot N120328 is the most kinetic-like implosion, where $T_i = 11.4$ keV, $n_i \sim 7 \times 10^{22}$ cm^{-3}, and Z = 1, resulting in a λ_{ii} of ~ 50 μm. In this case, $R_{shell} = 180$ μm and N_K is ~ 0.3. Parameters used to calculate the experimentally-inferred Knudsen numbers are summarized in Table V, and YOC values are shown as a function of the experimentally-inferred Knudsen numbers in Figure 8. For both DD and D^3He yields, each set of simulations shows a trend of decreasing YOC with increasing N_K. For the NLET-CBET DRACO simulations, DD YOC ~ 1 for N_K ~ 0.04, while DD YOC ~ 0.4 at N_K ~ 0.3. As the DRACO hydrodynamics code does not account for kinetic effects, ion mean free path effects such as enhanced ion diffusion and Knudsen reactivity reduction due to modification of the ion distribution function[63–65] may account for this trend. It has been shown previously that kinetic effects reduce shock yields in exploding pushers, and do so more strongly with increasing Knudsen number.[12]

TABLE V. Estimates of ion density, ion temperature, mean ion charge, minimum shell radius, Maxwellian-averaged mean free path for ion-ion collisions, and Knudsen number. The ion-ion mean free path and, therefore, the Knudsen number, varies largely as a consequence of variations in ion temperature and in gas composition ($\langle Z \rangle$). In the D^3He-filled implosions, a small, known amount of ^3He leaks out of the capsule before it is shot, reducing $\langle Z \rangle$ to slightly below 1.5.

NIF Shot #	n_i (cm^{-3})	T_i (keV)	$\langle Z \rangle$	λ_{ii} (μm)	R_{shell} (μm)	N_K
N110131	11×10^{22}	5.4	1	9	89	0.1
N110722	6×10^{22}	10.8	1.44	12	115	0.1
N120328	7×10^{22}	11.4	1	50	182	0.3
N121128	7×10^{22}	8.0	1.47	6	150	0.04
N130129	11×10^{22}	4.0	1	5	94	0.05

For these largely shock-driven implosions, hydrodynamic mix at the fuel-shell interface is very unlikely to explain the trend of decreasing YOC with increasing Knudsen number. In order for mix to explain this trend, the most "kinetic" implosion, N120328, would have to be the most susceptible to mix, to be driven by compression more so than the other implosions. However, by virtue
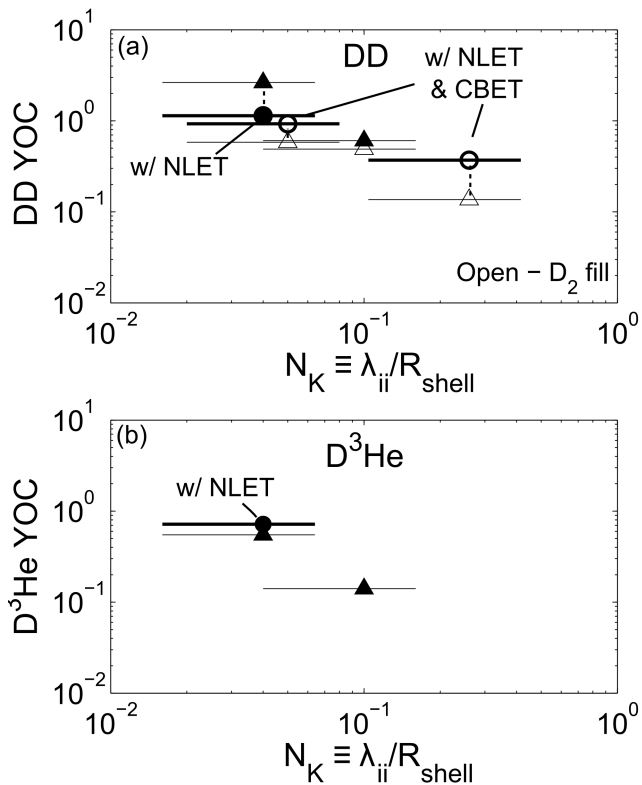
FIG. 8. (a) DD and (b) D^3He YOC as a function of the Knudsen number (N_K)– the ratio of ion-ion mean free path (λ_{ii}) to minimum shell radius (R_{shell}). The triangles represent the comparison of data to nominal DRACO simulations, while the circles represent the comparison of data to DRACO simulations that have included non-local electron transport (NLET) and cross-beam energy transfer (CBET). When both nominal and NLET/CBET DRACO simulations have been performed for a given experiment, those points are connected by a dotted vertical line. The trend of decreasing YOC with increasing λ_{ii}/R_{shell} across all simulations suggests that kinetic effects are starting to impact the experimental yields.

TABLE VI. Estimates of ion density, ion temperature, mean ion charge, gas composition, Maxwellian-averaged mean free path for ion-ion collisions, and Knudsen number after shock convergence for: a strongly-kinetic exploding pusher on OMEGA from Rosenberg et al.;[12] a NIF direct-drive exploding pusher from this study; a strongly hydrodynamic-like indirect-drive exploding pusher on NIF from Le Pape et al.;[15], and an ignition-relevant indirect-drive implosion. The parameters corresponding to hot-spot conditions during the compression phase of an indirect-drive ignition implosion are also presented. The three exploding pusher cases span the regimes of strongly kinetic to strongly hydrodynamic-like. For the exploding pushers, the ion density and ion temperature are estimated from experimental measurements, while for the NIF indirect-drive ignition-relevant shock phase case, they are taken from hydrodynamic simulations of a surrogate implosion, near the center of the implosion immediately after shock convergence. The NIF indirect-drive ignition compression phase case is an estimate based on recent NIF experiments.[69] In both shot N120328 (the most kinetic-like of the NIF direct-drive exploding pushers presented here) and the shock phase of the NIF indirect-drive ignition-relevant implosion, $\lambda_{ii} \sim 50$ μm, which approaches the size of the burn region (~ 100 μm) in the ignition-relevant case ($N_K \sim 0.5$).

Implosion	n_i (cm^{-3})	T_i (keV)	$\langle Z \rangle$	Fuel	λ_{ii} (μm)	N_K
Rosenberg et al.	4×10^{21}	28	1.5	D^3He	900	10
N120328	7×10^{22}	11.4	1	DD	50	0.3
Le Pape et al.	3×10^{23}	3.5	1	DD	2	0.01
NIF Ignition (shock phase)	$\sim6\times10^{22}$	~10	1	DT	~45	~0.5
NIF Ignition (compr. phase)	10^{25}	4	1	DT	0.1	0.002

of having the highest measured DD-burn-averaged ion temperature – a strong signature of shock heating – it is likely that this shot is the most predominantly shock-driven, with fusion reactions generated along the shock rebound trajectory. It is therefore unlikely that this shot is preferentially susceptible to the deleterious effects of mix, and in fact it may be even less compressively-driven (and less susceptible to mix) than the other implosions in this study.[66] Preliminary 2D ARES simulations[67] that include a KL mix model[68] indicate that mix does not have a significant impact on simulated yields and that a trend of lower yield-over-simulated (YOS) for higher-N_K implosions persists. As mix does not appear able to account for the trend of decreasing YOC with increasing Knudsen number, ion kinetic effects, rather than mix, are inferred as the likely explanation.

The results of these NIF direct-drive exploding-pusher experiments fit within the context of those previously observed in direct-drive exploding pushers at higher N_K on OMEGA[12] and indirect-drive exploding pushers at much lower N_K on NIF.[15] Table VI shows the ion-ion mean free path and Knudsen number in each of these exploding pusher experiments, as well as shortly (~100 ps) after shock convergence in a surrogate, indirect-drive ignition-relevant implosion on NIF and during the peak compression phase of a NIF ignition-relevant implosion. In the OMEGA experiments (Rosenberg et al.),[12] the YOC was found to be a strong inverse function of N_K for $0.3 \lesssim N_K \lesssim 10$; in the NIF indirect-drive exploding pushers (Le Pape et al.),[15] YOC~1, near-perfect agreement with hydrodynamic models, was obtained on implosions with $N_K \sim 0.01$. The present NIF direct-drive exploding-pusher experiments span the N_K space in between those extremes and demonstrate that the deviation from hydrodynamic models becomes noticeable between $0.1 \lesssim N_K \lesssim 0.3$. This trend in YOC as a function of N_K over the different experimental campaigns is illustrated in Figure 1, showing a consistent picture of the onset of ion kinetic effects with increasing Knudsen number, despite radically different drive conditions. Notably, the most kinetic-like implosion among the NIF PDD exploding-

pusher data set overlaps in both N_K and YOC with the most hydrodynamic-like implosion in the OMEGA direct-drive exploding-pusher set.

Additionally, in both the more kinetic-like N120328 exploding-pusher example and the NIF indirect-drive ignition case, $\lambda_{ii} \sim 50$ μm after shock convergence, an appreciable fraction of the size of the hot spot. The Knudsen number of ~ 0.5 after shock convergence in the NIF indirect-drive ignition implosion applies to NIF polar-direct-drive ignition-relevant implosions as well, and underestimates the Knudsen number after shock convergence in cryogenic layered implosions on OMEGA. Under those conditions, ion diffusion may significantly alter the density profiles, and Knudsen layer effects may allow the higher-energy ions to escape the hot-spot region.

In a NIF ignition implosion, the continued shell convergence after shock rebound greatly increases the fuel ion density, reducing λ_{ii} and N_K and producing much more hydrodynamic-like conditions around peak compression. The question that will be addressed in the future is: could the kinetic-like conditions during the shock convergence phase, including multiple-ion effects,[70,71] have any lingering manifestations and effects on the subsequent compression phase, which is strongly hydrodynamic-like (as shown in Table VI)? Ongoing and future experiments will explore this open question. Measurements of the relative and absolute timing of shock and compression bang time on surrogate implosions the NIF, as have been recently obtained and will be obtained routinely in the future,[72] may shed light on this issue.

Further studies will investigate aspects of the shock convergence phase of ICF implosions using exploding pushers, where ion kinetic effects are likely to be important. Yield anomalies in mixed-fuel exploding pushers will be explored and may elucidate species separation during shock convergence.[71] A comparison of exploding-pusher data to a hybrid kinetic treatment like that of Larroche[11,73] is an important continuation of this study. That theoretical work shows that kinetic simulations produce weaker and smoother profiles of temperatures and density near shock-bang time than hydrodynamic simulations, as the shock front is broadened to $\sim \lambda_{ii}$. Exploding-pusher experiments conducted in the indirect-drive configuration[15] will continue to be studied. These experiments in particular more closely approximate the process of shock convergence and shock burn as it occurs in NIF indirect-drive implosions.

V. CONCLUSIONS

In order to fully exploit diagnostic development shots at the NIF, ride-along measurements of fusion yield, fuel ion temperature, ρR, convergence, and bang time have been presented for polar-direct-drive, D_2 and D^3He exploding-pusher implosions. These data are used to probe the physics of the shock convergence phase of implosions relevant both to shock-driven, exploding-pusher implosions and to ablatively-driven implosions, when ion kinetic effects can be important. The data have been compared to 2D DRACO hydrodynamic simulations and show a notable trend of decreasing YOC with increasing Knudsen number ($N_K \equiv \lambda_{ii}/R_{shell}$). This trend is suggestive of ion kinetic effects, and is consistent with the results of previous experiments at much higher and much lower Knudsen number, even though these implosions used different capsules and polar-direct-drive illumination. This work also motivates the continued development of kinetic models of ICF implosions, which may be especially pertinent at the high-temperature, moderate-density conditions present at shock burn in both exploding pushers and the shock-convergence phase of ablatively-driven implosions.

[1] H. Brysk and P. Hammerling, Phys. Rev. Lett. **34**, 502 (1975).
[2] E. K. Storm, H. G. Ahlstrom, M. J. Boyle, D. E. Campbell, L. W. Coleman, S. S. Glaros, H. N. Kornblum, R. A. Lerche, D. R. MacQuigg, D. W. Phillion, F. Rainer, R. Rienecker, V. C. Rupert, V. W. Slivinsky, D. R. Speck, C. D. Swift, and K. G. Tirsell, Phys. Rev. Lett. **40**, 1570 (1978).
[3] M. D. Rosen and J. H. Nuckolls, Physics of Fluids **22** (1979).
[4] B. Ahlborn and M. H. Key, Plasma Physics **23**, 435 (1981).
[5] S. H. Glenzer, D. A. Callahan, A. J. MacKinnon, J. L. Kline, G. Grim, E. T. Alger, R. L. Berger, L. A. Bernstein, R. Betti, D. L. Bleuel, T. R. Boehly, D. K. Bradley, S. C. Burkhart, R. Burr, J. A. Caggiano, C. Castro, D. T. Casey, C. Choate, D. S. Clark, P. Celliers, C. J. Cerjan, G. W. Collins, E. L. Dewald, P. DiNicola, J. M. DiNicola, L. Divol, S. Dixit, T. Döppner, R. Dylla-Spears, E. Dzenitis, M. Eckart, G. Erbert, D. Farley, J. Fair, D. Fittinghoff, M. Frank, L. J. A. Frenje, S. Friedrich, D. T. Casey, M. Gatu Johnson, C. Gibson, E. Giraldez, V. Glebov, S. Glenn, N. Guler, S. W. Haan, B. J. Haid, B. A. Hammel, A. V. Hamza, C. A. Haynam, G. M. Heestand, M. Hermann, H. W. Hermann, D. G. Hicks, D. E. Hinkel, J. P. Holder, D. M. Holunda, J. B. Horner, W. W. Hsing, H. Huang, N. Izumi, M. Jackson, O. S. Jones, D. H. Kalantar, R. Kauffman, J. D. Kilkenny, R. K. Kirkwood, J. Klingmann, T. Kohut, J. P. Knauer, J. A. Koch, B. Kozioziemki, G. A. Kyrala, A. L. Kritcher, J. Kroll, K. La Fortune, L. Lagin, O. L. Landen, D. W. Larson, D. LaTray, R. J. Leeper, S. Le Pape, J. D. Lindl, R. Lowe-Webb, T. Ma, J. McNaney, A. G. MacPhee, T. N. Malsbury, E. Mapoles, C. D. Marshall, N. B. Meezan, F. Merrill, P. Michel, J. D. Moody, A. S. Moore, M. Moran, K. A. Moreno, D. H. Munro, B. R. Nathan, A. Nikroo, R. E. Olson, C. D. Orth, A. E. Pak, P. K. Patel, T. Parham, R. Petrasso, J. E. Ralph, H. Rinderknecht, S. P. Regan, H. F. Robey, J. S. Ross, M. D. Rosen, R. Sacks, J. D. Salmonson, R. Saunders, J. Sater, C. Sangster, M. B. Schneider, F. H. Séguin, M. J. Shaw, B. K. Spears, P. T. Springer, W. Stoeffl, L. J. Suter, C. A. Thomas, R. Tommasini, R. P. J. Town, C. Walters, S. Weaver, S. V. Weber, P. J.

Wegner, P. K. Whitman, K. Widmann, C. C. Widmayer, C. H. Wilde, D. C. Wilson, B. Van Wonterghem, B. J. MacGowan, L. J. Atherton, M. J. Edwards, and E. I. Moses, Physics of Plasmas **19**, 056318 (2012).

[6] H. F. Robey, P. M. Celliers, J. L. Kline, A. J. Mackinnon, T. R. Boehly, O. L. Landen, J. H. Eggert, D. Hicks, S. Le Pape, D. R. Farley, M. W. Bowers, K. G. Krauter, D. H. Munro, O. S. Jones, J. L. Milovich, D. Clark, B. K. Spears, R. P. J. Town, S. W. Haan, S. Dixit, M. B. Schneider, E. L. Dewald, K. Widmann, J. D. Moody, T. D. Döppner, H. B. Radousky, A. Nikroo, J. J. Kroll, A. V. Hamza, J. B. Horner, S. D. Bhandarkar, E. Dzenitis, E. Alger, E. Giraldez, C. Castro, K. Moreno, C. Haynam, K. N. LaFortune, C. Widmayer, M. Shaw, K. Jancaitis, T. Parham, D. M. Holunga, C. F. Walters, B. Haid, T. Malsbury, D. Trummer, K. R. Coffee, B. Burr, L. V. Berzins, C. Choate, S. J. Brereton, S. Azevedo, H. Chandrasekaran, S. Glenzer, J. A. Caggiano, J. P. Knauer, J. A. Frenje, D. T. Casey, M. Gatu Johnson, F. H. Séguin, B. K. Young, M. J. Edwards, B. M. Van Wonterghem, J. Kilkenny, B. J. MacGowan, J. Atherton, J. D. Lindl, D. D. Meyerhofer, and E. Moses, Phys. Rev. Lett. **108**, 215004 (2012).

[7] D. G. Hicks, N. B. Meezan, E. L. Dewald, A. J. Mackinnon, R. E. Olson, D. A. Callahan, T. D"oppner, L. R. Benedetti, D. K. Bradley, P. M. Celliers, D. S. Clark, P. Di Nicola, S. N. Dixit, E. G. Dzenitis, J. E. Eggert, D. R. Farley, J. A. Frenje, S. M. Glenn, S. H. Glenzer, A. V. Hamza, R. F. Heeter, J. P. Holder, N. Izumi, D. H. Kalantar, S. F. Khan, J. L. Kline, J. J. Kroll, G. A. Kyrala, T. Ma, A. G. MacPhee, J. M. McNaney, J. D. Moody, M. J. Moran, B. R. Nathan, A. Nikroo, Y. P. Opachich, R. D. Petrasso, R. R. Prasad, J. E. Ralph, H. F. Robey, H. G. Rinderknecht, J. R. Rygg, J. D. Salmonson, M. B. Schneider, N. Simanovskaia, B. K. Spears, R. Tommasini, K. Widmann, A. B. Zylstra, G. W. Collins, O. L. Landen, J. D. Kilkenny, W. W. Hsing, B. J. MacGowan, L. J. Atherton, and M. J. Edwards, Physics of Plasmas **19**, 122702 (2012).

[8] A. J. Mackinnon, J. L. Kline, S. N. Dixit, S. H. Glenzer, M. J. Edwards, D. A. Callahan, N. B. Meezan, S. W. Haan, J. D. Kilkenny, T. Döppner, D. R. Farley, J. D. Moody, J. E. Ralph, B. J. MacGowan, O. L. Landen, H. F. Robey, T. R. Boehly, P. M. Celliers, J. H. Eggert, K. Krauter, G. Frieders, G. F. Ross, D. G. Hicks, R. E. Olson, S. V. Weber, B. K. Spears, J. D. Salmonsen, P. Michel, L. Divol, B. Hammel, C. A. Thomas, D. S. Clark, O. S. Jones, P. T. Springer, C. J. Cerjan, G. W. Collins, V. Y. Glebov, J. P. Knauer, C. Sangster, C. Stoeckl, P. McKenty, J. M. McNaney, R. J. Leeper, C. L. Ruiz, G. W. Cooper, A. G. Nelson, G. G. A. Chandler, K. D. Hahn, M. J. Moran, M. B. Schneider, N. E. Palmer, R. M. Bionta, E. P. Hartouni, S. LePape, P. K. Patel, N. Izumi, R. Tommasini, E. J. Bond, J. A. Caggiano, R. Hatarik, G. P. Grim, F. E. Merrill, D. N. Fittinghoff, N. Guler, O. Drury, D. C. Wilson, H. W. Herrmann, W. Stoeffl, D. T. Casey, M. G. Johnson, J. A. Frenje, R. D. Petrasso, A. Zylstra, H. Rinderknecht, D. H. Kalantar, J. M. Dzenitis, P. Di Nicola, D. C. Eder, W. H. Courdin, G. Gururangan, S. C. Burkhart, S. Friedrich, D. L. Blueuel, l. A. Bernstein, M. J. Eckart, D. H. Munro, S. P. Hatchett, A. G. Macphee, D. H. Edgell, D. K. Bradley, P. M. Bell, S. M. Glenn, N. Simanovskaia, M. A. Barrios, R. Benedetti, G. A. Kyrala, R. P. J. Town, E. L. Dewald, J. L. Milovich, K. Widmann, A. S. Moore, G. LaCaille, S. P. Regan, L. J. Suter, B. Felker, R. C. Ashabranner, M. C. Jackson, R. Prasad, M. J. Richardson, T. R. Kohut, P. S. Datte, G. W. Krauter, J. J. Klingman, R. F. Burr, T. A. Land, M. R. Hermann, D. A. Latray, R. L. Saunders, S. Weaver, S. J. Cohen, L. Berzins, S. G. Brass, E. S. Palma, R. R. Lowe-Webb, G. N. McHalle, P. A. Arnold, L. J. Lagin, C. D. Marshall, G. K. Brunton, D. G. Mathisen, R. D. Wood, J. R. Cox, R. B. Ehrlich, K. M. Knittel, M. W. Bowers, R. A. Zacharias, B. K. Young, J. P. Holder, J. R. Kimbrough, T. Ma, K. N. La Fortune, C. C. Widmayer, M. J. Shaw, G. V. Erbert, K. S. Jancaitis, J. M. DiNicola, C. Orth, G. Heestand, R. Kirkwood, C. Haynam, P. J. Wegner, P. K. Whitman, A. Hamza, E. G. Dzenitis, R. J. Wallace, S. D. Bhandarkar, T. G. Parham, R. Dylla-Spears, E. R.

Mapoles, B. J. Kozioziemski, J. D. Sater, C. F. Walters, B. J. Haid, J. Fair, A. Nikroo, E. Giraldez, K. Moreno, B. Vanwonterghem, R. L. Kauffman, S. Batha, D. W. Larson, R. J. Fortner, D. H. Schneider, J. D. Lindl, R. W. Patterson, L. J. Atherton, and E. I. Moses, Phys. Rev. Lett. **108**, 215005 (2012).

[9] M. J. Edwards, P. K. Patel, J. D. Lindl, L. J. Atherton, S. H. Glenzer, S. W. Haan, J. D. Kilkenny, O. L. Landen, E. I. Moses, A. Nikroo, R. Petrasso, T. C. Sangster, P. T. Springer, S. Batha, R. Benedetti, L. Bernstein, R. Betti, D. L. Bleuel, T. R. Boehly, D. K. Bradley, J. A. Caggiano, D. A. Callahan, P. M. Celliers, C. J. Cerjan, K. C. Chen, D. S. Clark, G. W. Collins, E. L. Dewald, L. Divol, S. Dixit, T. Doeppner, D. H. Edgell, J. E. Fair, M. Farrell, R. J. Fortner, J. Frenje, M. G. Gatu Johnson, E. Giraldez, V. Y. Glebov, G. Grim, B. A. Hammel, A. V. Hamza, D. R. Harding, S. P. Hatchett, N. Hein, H. W. Herrmann, D. Hicks, D. E. Hinkel, M. Hoppe, W. W. Hsing, N. Izumi, B. Jacoby, O. S. Jones, D. Kalantar, R. Kauffman, J. L. Kline, J. P. Knauer, J. A. Koch, B. J. Kozioziemski, G. Kyrala, K. N. LaFortune, S. L. Pape, R. J. Leeper, R. Lerche, T. Ma, B. J. MacGowan, A. J. MacKinnon, A. Macphee, E. R. Mapoles, M. M. Marinak, M. Mauldin, P. W. McKenty, M. Meezan, P. A. Michel, J. Milovich, J. D. Moody, M. Moran, D. H. Munro, C. L. Olson, K. Opachich, A. E. Pak, T. Parham, H.-S. Park, J. E. Ralph, S. P. Regan, B. Remington, H. Rinderknecht, H. F. Robey, M. Rosen, S. Ross, J. D. Salmonson, J. Sater, D. H. Schneider, F. H. Sguin, S. M. Sepke, D. A. Shaughnessy, V. A. Smalyuk, B. K. Spears, C. Stoeckl, W. Stoeffl, L. Suter, C. A. Thomas, R. Tommasini, R. P. Town, S. V. Weber, P. J. Wegner, K. Widman, M. Wilke, D. C. Wilson, C. B. Yeamans, and A. Zylstra, Physics of Plasmas **20**, 070501 (2013).

[10] T. R. Dittrich, O. A. Hurricane, D. A. Callahan, E. L. Dewald, T. Döppner, D. E. Hinkel, L. F. Berzak Hopkins, S. Le Pape, T. Ma, J. L. Milovich, J. C. Moreno, P. K. Patel, H.-S. Park, B. A. Remington, J. D. Salmonson, and J. L. Kline, Phys. Rev. Lett. **112**, 055002 (2014).

[11] O. Larroche, The European Physical Journal D - Atomic, Molecular, Optical and Plasma Physics **27**, 131 (2003).

[12] M. J. Rosenberg, H. G. Rinderknecht, N. M. Hoffman, P. A. Amendt, S. Atzeni, A. B. Zylstra, C. K. Li, F. H. Séguin, H. Sio, M. G. Johnson, J. A. Frenje, R. D. Petrasso, V. Y. Glebov, C. Stoeckl, W. Seka, F. J. Marshall, J. A. Delettrez, T. C. Sangster, R. Betti, V. N. Goncharov, D. D. Meyerhofer, S. Skupsky, C. Bellei, J. Pino, S. C. Wilks, G. Kagan, K. Molvig, and A. Nikroo, Phys. Rev. Lett. **112**, 185001 (2014).

[13] H. G. Rinderknecht, H. Sio, C. K. Li, A. B. Zylstra, M. J. Rosenberg, P. Amendt, J. Delettrez, C. Bellei, J. A. Frenje, M. Gatu Johnson, F. H. Séguin, R. D. Petrasso, R. Betti, V. Y. Glebov, D. D. Meyerhofer, T. C. Sangster, C. Stoeckl, O. Landen, V. A. Smalyuk, S. Wilks, A. Greenwood, and A. Nikroo, Phys. Rev. Lett. **112**, 135001 (2014).

[14] S. Atzeni, Computer Physics Communications **43**, 107 (1986).

[15] S. Le Pape, L. Divol, L. Berzak Hopkins, A. Mackinnon, N. Meezan, D. Casey, J. Frenje, H. Herrmann, J. McNaney, T. Ma, K. Widmann, A. Pak, G. Grimm, J. Knauer, R. Petrasso, A. Zylstra, H. Rinderknecht, M. Rosenberg, M. Gatu Johnson, and J. D. Kilkenny, Phys. Rev. Lett. **112**, 225002 (2014).

[16] S. Skupsky, J. A. Marozas, R. S. Craxton, R. Betti, T. J. B. Collins, J. A. Delettrez, V. N. Goncharov, P. W. McKenty, P. B. Radha, T. R. Boehly, J. P. Knauer, F. J. Marshall, D. R. Harding, J. D. Kilkenny, D. D. Meyerhofer, T. C. Sangster, and R. L. McCrory, Physics of Plasmas **11**, 2763 (2004).

[17] D. L. Bleuel, C. B. Yeamans, L. A. Bernstein, R. M. Bionto, J. A. Caggiano, D. T. Casey, G. W. Cooper, O. B. Drury, J. A. Frenje, C. A. Hagmann, R. Hatarik, J. P. Knauer, M. G. Johnson, K. M. Knittel, R. J. Leeper, J. M. McNaney, M. Moran, C. L. Ruiz, and D. H. G. Schneider, Rev. Sci. Inst. **83**, 10D313 (2012).

[18] D. T. Casey, J. A. Frenje, M. G. Johnson, F. H. Séguin, C. K. Li, R. D. Petrasso, V. Y. Glebov, J. Katz, D. D. Meyerhofer, T. C. Sangster, M. Shoup, J. Ulreich, R. C. Ashabranner, R. M. Bionta, A. C. Carpenter, B. Felker, H. Y. Khater, S. LePape,

A. MacKinnon, M. A. McKernan, M. Moran, J. R. Rygg, M. F. Yeoman, R. Zacharias, R. J. Leeper, K. Fletcher, M. Farrell, D. Jaslon, J. Kilkenny, and R. Pagulo, Rev. Sci. Inst. **84**, 043506 (2013).

[19] M. J. Rosenberg, A. B. Zylstra, J. A. Frenje, H. G. Rinderknecht, M. Gatu Johnson, C. J. Waugh, F. H. Sguin, H. Sio, N. Sinenian, C. K. Li, R. D. Petrasso, V. Y. Glebov, M. Hohenberger, C. Stoeckl, T. C. Sangster, C. B. Yeamans, S. LePape, A. J. Mackinnon, R. M. Bionta, B. Talison, D. T. Casey, O. L. Landen, M. J. Moran, R. A. Zacharias, J. D. Kilkenny, and A. Nikroo, Review of Scientific Instruments **85**, 103504 (2014).

[20] P. B. Radha, V. N. Goncharov, T. J. B. Collins, J. A. Delettrez, Y. Elbaz, V. Y. Glebov, R. L. Keck, D. E. Keller, J. P. Knauer, J. A. Marozas, F. J. Marshall, P. W. McKenty, D. D. Meyerhofer, S. P. Regan, T. C. Sangster, D. Shvarts, S. Skupsky, Y. Srebro, R. P. J. Town, and C. Stoeckl, Physics of Plasmas **12**, 032702 (2005).

[21] The total ion mean free path in a multiple-ion plasma is based on the total collision rate of a test ion on each population of ions (for example: D on D + D on ^{3}He; ^{3}He on D + ^{3}He on ^{3}He). In terms of mean free paths, $\lambda_{Di}^{-1} = \lambda_{DD}^{-1} + \lambda_{D^3He}^{-1}$; $\lambda_{^3Hei}^{-1} = \lambda_{^3HeD}^{-1} + \lambda_{^3He^3He}^{-1}$. The overall ion mean free path is taken as the geometric mean, $\lambda_{ii} = \sqrt{\lambda_{Di}\lambda_{^3Hei}}$.

[22] T. C. Sangster, V. N. Goncharov, R. Betti, P. B. Radha, T. R. Boehly, D. T. Casey, T. J. B. Collins, R. S. Craxton, J. A. Delettrez, D. H. Edgell, R. Epstein, C. J. Forrest, J. A. Frenje, D. H. Froula, M. Gatu-Johnson, Y. Y. Glebov, D. R. Harding, M. Hohenberger, S. X. Hu, I. V. Igumenshchev, R. Janezic, J. H. Kelly, T. J. Kessler, C. Kingsley, T. Z. Kosc, J. P. Knauer, S. J. Loucks, J. A. Marozas, F. J. Marshall, A. V. Maximov, R. L. McCrory, P. W. McKenty, D. D. Meyerhofer, D. T. Michel, J. F. Myatt, R. D. Petrasso, S. P. Regan, W. Seka, W. T. Shmayda, R. W. Short, A. Shvydky, S. Skupsky, J. M. Soures, C. Stoeckl, W. Theobald, V. Versteeg, B. Yaakobi, and J. D. Zuegel, Physics of Plasmas **20**, 056317 (2013).

[23] G. H. Miller, E. I. Moses, and C. R. Wuest, Optical Engineering **43**, 2841 (2004).

[24] J. Delettrez, R. Epstein, M. C. Richardson, P. A. Jaanimagi, and B. L. Henke, Phys. Rev. A **36**, 3926 (1987).

[25] J. Delettrez, Can. J. Phys. **64**, 932 (1986).

[26] T. R. Boehly, D. L. Brown, R. S. Craxton, R. L. Keck, J. P. Knauer, J. H. Kelly, T. J. Kessler, S. A. Kumpan, S. J. Loucks, S. A. Letzring, F. J. Marshall, R. L. McCrory, S. F. B. Morse, W. Seka, J. M. Soures, and C. P. Verdon, Opt. Commun. **133**, 495 (1997).

[27] J. A. Marozas, F. J. Marshall, R. S. Craxton, I. V. Igumenshchev, S. Skupsky, M. J. Bonino, T. J. B. Collins, R. Epstein, V. Y. Glebov, D. Jacobs-Perkins, J. P. Knauer, T. C. Sangster, W. Seka, and V. A. Smalyuk, Phys. Plasmas **13**, 056311 (2006).

[28] P. B. Radha, F. J. Marshall, J. A. Marozas, A. Shvydky, I. Gabalski, T. R. Boehly, T. J. B. Collins, R. S. Craxton, D. H. Edgell, R. Epstein, J. A. Frenje, D. H. Froula, V. N. Goncharov, M. Hohenberger, R. L. McCrory, P. W. McKenty, D. D. Meyerhofer, R. D. Petrasso, T. C. Sangster, and S. Skupsky, Phys. Plasmas **20**, 056306 (2013).

[29] P. W. McKenty, T. C. Sangster, M. Alexander, R. Betti, R. S. Craxton, J. A. Delettrez, L. Elasky, R. Epstein, A. Frank, V. Y. Glebov, V. N. Goncharov, D. R. Harding, S. Jin, J. P. Knauer, R. L. Keck, S. J. Loucks, L. D. Lund, R. L. McCrory, F. J. Marshall, D. D. Meyerhofer, S. P. Regan, P. B. Radha, S. Roberts, W. Seka, S. Skupsky, V. A. Smalyuk, J. M. Soures, K. A. Thorp, M. Wozniak, J. A. Frenje, C. K. Li, R. D. Petrasso, F. H. Séguin, K. A. Fletcher, S. Padalino, C. Freeman, N. Izumi, J. A. Koch, R. A. Lerche, M. J. Moran, T. W. Phillips, G. J. Schmid, and C. Sorce, Phys. Plasmas **11**, 2790 (2004).

[30] F. J. Marshall, R. S. Craxton, J. A. Delettrez, D. H. Edgell, L. M. Elasky, R. Epstein, V. Y. Glebov, V. N. Goncharov, D. R. Harding, R. Janezic, R. L. Keck, J. D. Kilkenny, J. P. Knauer, S. J. Loucks, L. D. Lund, R. L. McCrory, P. W. McKenty, D. D.

[31] S. X. Hu, V. N. Goncharov, P. B. Radha, J. A. Marozas, S. Skupsky, T. R. Boehly, T. C. Sangster, D. D. Meyerhofer, and R. L. McCrory, Phys. Plasmas **17**, 102706 (2010).

Meyerhofer, P. B. Radha, S. P. Regan, T. C. Sangster, W. Seka, V. A. Smalyuk, J. M. Soures, C. Stoeckl, and S. Skupsky, Phys. Plasmas **12**, 056302 (2005).

[32] V. N. Goncharov, T. C. Sangster, R. Betti, T. R. Boehly, M. J. Bonino, T. J. B. Collins, R. S. Craxton, J. A. Delettrez, D. H. Edgell, R. Epstein, R. K. Follett, C. J. Forrest, D. H. Froula, V. Yu. Glebov, D. R. Harding, R. J. Henchen, S. X. Hu, I. V. Igumenshchev, R. Janezic, J. H. Kelly, T. J. Kessler, T. Z. Kosc, S. J. Loucks, J. A. Marozas, F. J. Marshall, A. V. Maximov, R. L. McCrory, P. W. McKenty, D. D. Meyerhofer, D. T. Michel, J. F. Myatt, R. Nora, P. B. Radha, S. P. Regan, W. Seka, W. T. Shmayda, R. W. Short, A. Shvydky, S. Skupsky, C. Stoeckl, B. Yaakobi, J. A. Frenje, M. Gatu-Johnson, R. D. Petrasso, and D. T. Casey, Physics of Plasmas **21**, 056315 (2014).

[33] A. Sunahara, J. A. Delettrez, C. Stoeckl, R. W. Short, and S. Skupsky, Phys. Rev. Lett. **91**, 095003 (2003).

[34] G. P. Schurtz, P. D. Nicola, and M. Busquet, Physics of Plasmas **7** (2000).

[35] P. Michel, L. Divol, E. A. Williams, S. Weber, C. A. Thomas, D. A. Callahan, S. W. Haan, J. D. Salmonson, S. Dixit, D. E. Hinkel, M. J. Edwards, B. J. MacGowan, J. D. Lindl, S. H. Glenzer, and L. J. Suter, Phys. Rev. Lett. **102**, 025004 (2009).

[36] V. Y. Glebov, C. Stoeckl, T. C. Sangster, S. Roberts, G. J. Schmid, R. A. Lerche, and M. J. Moran, Review of Scientific Instruments **75**, 3559 (2004).

[37] V. Y. Glebov, D. D. Meyerhofer, T. C. Sangster, C. Stoeckl, S. Roberts, C. A. Barrera, J. R. Celeste, C. J. Cerjan, L. S. Dauffy, D. C. Eder, R. L. Griffith, S. W. Haan, B. A. Hammel, S. P. Hatchett, N. Izumi, J. R. Kimbrough, J. A. Koch, O. L. Landen, R. A. Lerche, B. J. MacGowan, M. J. Moran, E. W. Ng, T. W. Phillips, P. M. Song, R. Tommasini, B. K. Young, S. E. Caldwell, G. P. Grim, S. C. Evans, J. M. Mack, T. J. Sedillo, M. D. Wilke, D. C. Wilson, C. S. Young, D. Casey, J. A. Frenje, C. K. Li, R. D. Petrasso, F. H. Séguin, J. L. Bourgade, L. Disdier, M. Houry, I. Lantuejoul, O. Landoas, G. A. Chandler, G. W. Cooper, R. J. Leeper, R. E. Olson, C. L. Ruiz, M. A. Sweeney, S. P. Padalino, C. Horsfield, and B. A. Davis, Rev. Sci. Inst. **77**, 10E715 (2006).

[38] F. H. Séguin, J. A. Frenje, C. K. Li, D. G. Hicks, S. Kurebayashi, J. R. Rygg, B.-E. Schwartz, R. D. Petrasso, S. Roberts, J. M. Soures, D. D. Meyerhofer, T. C. Sangster, J. P. Knauer, C. Sorce, V. Y. Glebov, C. Stoeckl, T. W. Phillips, R. J. Leeper, K. Fletcher, and S. Padalino, Review of Scientific Instruments **74**, 975 (2003).

[39] On shot N130129, the CR-39-based DD-proton yield measurement was used to roughly confirm the DD-neutron yield measurement.

[40] F. H. Séguin, N. Sinenian, M. Rosenberg, A. Zylstra, M. J.-E. Manuel, H. Sio, C. Waugh, H. G. Rinderknecht, M. G. Johnson, J. Frenje, C. K. Li, R. Petrasso, T. C. Sangster, and S. Roberts, Review of Scientific Instruments **83**, 10D908 (2012).

[41] A. B. Zylstra, J. A. Frenje, F. H. Séguin, M. J. Rosenberg, H. G. Rinderknecht, M. G. Johnson, D. T. Casey, N. Sinenian, M. J.-E. Manuel, C. J. Waugh, H. W. Sio, C. K. Li, R. D. Petrasso, S. Friedrich, K. Knittel, R. Bionta, M. McKernan, D. Callahan, G. W. Collins, E. Dewald, T. Doppner, M. J. Edwards, S. Glenzer, D. G. Hicks, O. L. Landen, R. London, A. Mackinnon, N. Meezan, R. R. Prasad, J. Ralph, M. Richardson, J. R. Rygg, S. Sepke, S. Weber, R. Zacharias, E. Moses, J. Kilkenny, A. Nikroo, T. C. Sangster, V. Glebov, C. Stoeckl, R. Olson, R. J. Leeper, J. Kline, G. Kyrala, and D. Wilson, Review of Scientific Instruments **83**, 10D901 (2012).

[42] The total uncertainty of a given WRF yield measurement is $\sim\pm15\%$. As the yields are averages of 2-7 measurements, the overall yield uncertainty is reduced to $\sim\pm10\%$.

[43] D. G. Hicks, *Charged-Particle Spectroscopy: A New Window on Inertial Confinement Fusion*, Ph.D. thesis, Massachusetts Insti-

tute of Technology (1999).

[44] C. K. Li, D. G. Hicks, F. H. Séguin, J. A. Frenje, R. D. Petrasso, J. M. Soures, P. B. Radha, V. Y. Glebov, C. Stoeckl, D. R. Harding, J. P. Knauer, R. Kremens, F. J. Marshall, D. D. Meyerhofer, S. Skupsky, S. Roberts, C. Sorce, T. C. Sangster, T. W. Phillips, M. D. Cable, and R. J. Leeper, Phys. Plasmas **7**, 2578 (2000).

[45] Instrumental broadening for aluminum WRFs used at NIF is $\sigma \sim$130-170 keV, while a typical thermal Doppler width of the D^3He-p spectrum is $\sigma \sim$250 keV.

[46] This broadening arises from differential proton slowing due to different amounts of ρR across the burn duration and different path lengths for protons traversing the shell and sampling different effective amounts of ρR, and is modeled based on the measured ρR and simulated burn duration, assuming uniform proton emission throughout the fuel.

[47] T. J. Murphy, Physics of Plasmas **21**, 072701 (2014).

[48] Using the example of shot N121128, it is noted that for hypothetical random flow velocities of 50 μm/ns and 150 μm/ns, there is only a small impact on the ion temperature measurement. For a random flow velocity of 50 (150) μm/ns, the DD-n linewidth-inferred ion temperature measurement would be revised from 7.1 keV to 7.0 (6.2) keV, while the D^3He-p linewidth-inferred ion temperature measurement would be revised from 11.0 keV to 10.9 (9.8) keV. (If both DD-n and D^3He-p linewidth-inferred ion temperatures were the same value, e.g. 11 keV, the additional broadening to be added in quadrature to the fusion product spectra would be 25% greater for D^3He-p.).

[49] B. Appelbe and J. Chittenden, Plasma Physics and Controlled Fusion **53**, 045002 (2011).

[50] A. Inglebert, B. Canaud, and O. Larroche, EPL (Europhysics Letters) **107**, 65003 (2014).

[51] M. D. Cable and S. P. Hatchett, J. Appl. Phys. **62**, 2233 (1987).

[52] F. H. Séguin, C. K. Li, J. A. Frenje, D. G. Hicks, K. M. Green, S. Kurebayashi, R. D. Petrasso, J. M. Soures, D. D. Meyerhofer, V. Y. Glebov, P. B. Radha, C. Stoeckl, S. Roberts, C. Sorce, T. C. Sangster, T. W. Phillips, M. D. Cable, K. Fletcher, and S. Padalino, Phys. Plasmas **9**, 2525 (2002).

[53] S. Kurebayashi, J. A. Frenje, F. H. Séguin, J. R. Rygg, C. K. Li, R. D. Petrasso, V. Y. Glebov, J. A. Delettrez, T. C. Sangster, D. D. Meyerhofer, C. Stoeckl, J. M. Soures, P. A. Amendt, S. P. Hatchett, and R. E. Turner, Phys. Plasmas **12**, 032703 (2005).

[54] Because the average energy of the ^{3}He reactant ion in secondary D^3He reactions is much greater than the (thermal) reactant ion energy for primary D^3He reactions, the average birth energy of secondary D^3He-p is $\sim$300 keV higher than the average birth energy of a primary D^3He-p.

[55] The measurement of total ρR from energy downshift in the D^3He-p spectrum is sometimes complicated by the presence of radial electric fields around the capsule that cause an upshift in proton energy upon leaving the capsule,[74] such that the downshift-inferred total ρR is a lower limit on the actual ρR in the implosion. However, when the laser intensity is below $\sim 4 \times 10^{14}$ W/cm^2 or when the nuclear bang time is well after the end of the laser pulse, electric-field upshifts are diminished and the birth energy is well known. This is the case on five of the six experiments used in this study, with shot N120328 the only exception. On all other shots, bang time is $>$300 ps after the end of the laser pulse.

[56] The convergence ratio is related to the shell ρR as $C \sim \sqrt{\rho R_{sf}/(1-f)\rho R_{s0}}$, where ρR_{sf} (ρR_{s0}) is the final (initial) shell ρR and f is the fraction of shell material that has been blown off (beyond the initial shell radius). For an approximate blowoff fraction of $f = 0.6$ and $\rho R_{sf}/\rho R_{s0} \sim$10-20, $C \sim$5-7, consistent with $C \sim$6 inferred from the fuel ρR data.

[57] S. Glenn, J. Koch, D. K. Bradley, N. Izumi, P. Bell, G. Stone, R. Prasad, A. MacKinnon, P. Springer, O. L. Landen, and G. Kyrala, Rev. Sci. Inst. **81**, 10E539 (2010).

[58] G. A. Kyrala, S. Dixit, S. Glenzer, D. Kalantar, D. Bradley, N. Izumi, N. Meezan, O. L. Landen, D. Callahan, S. V. Weber, J. P. Holder, S. Glenn, M. J. Edwards, P. Bell, J. Kimbrough, J. Koch, R. Prasad, L. Suter, J. L. Kline, and J. Kilkenny, Rev.

[59] Sci. Inst. **81**, 10E316 (2010).

[59] Though there is some inconsistency between the convergence ratios inferred from the x-ray P0 measurements and the convergence ratios inferred from fuel ρR measurements, for the purpose of inferring an ion density in the later discussion, only the fuel ρR is used. The fuel ρR measurement is given greater weight due to the fact that it is a more direct probe of density.

[60] H. G. Rinderknecht, M. G. Johnson, A. B. Zylstra, N. Sinenian, M. J. Rosenberg, J. A. Frenje, C. J. Waugh, C. K. Li, F. H. Séguin, R. D. Petrasso, J. R. Rygg, J. R. Kimbrough, A. MacPhee, G. W. Collins, D. Hicks, A. Mackinnon, P. Bell, R. Bionta, T. Clancy, R. Zacharias, T. D'oppner, H. S. Park, S. LePape, O. Landen, N. Meezan, E. I. Moses, V. U. Glebov, C. Stoeckl, T. C. Sangster, R. Olson, J. Kline, and J. Kilkenny, Rev. Sci. Inst. **83**, 10D902 (2012).

[61] D. H. Edgell, D. K. Bradley, E. J. Bond, S. Burns, D. A. Callahan, J. Celeste, M. J. Eckhart, V. Y. Glebov, D. S. Hey, G. Lacaille, J. D. Kilkenny, J. Kimbrough, A. J. Mackinnon, J. Magoon, J. Parker, T. C. Sangster, M. J. S. III, C. Stoeckl, T. Thomas, and A. MacPhee, Rev. Sci. Inst. **83** (2012).

[62] Following the earlier discussion, the individual ion mean free paths $\lambda_{DD} \sim$52 μm, $\lambda_{D^3He} \sim$13 μm, $\lambda_{3HeD} \sim$16 μm, $\lambda_{3He^3He} \sim$4 μm, so that $\lambda_{Di} \sim$11 μm, $\lambda_{3Hei} \sim$3 μm and $\lambda_{ii} \sim$6 μm.

[63] A. G. Petschek and D. B. Henderson, Nucl. Fusion **19**, 1678 (1979).

[64] K. Molvig, N. M. Hoffman, B. J. Albright, E. M. Nelson, and R. B. Webster, Phys. Rev. Lett. **109**, 095001 (2012).

[65] B. J. Albright, K. Molvig, C.-K. Huang, A. N. Simakov, E. S. Dodd, N. M. Hoffman, G. Kagan, and P. F. Schmit, Physics of Plasmas **20**, 122705 (2013).

[66] In addition, a fall-line analysis[75] of 1D LILAC simulations, representing the worst-case application of hydrodynamic mix to a 1D model, indicates that mix fails to account for the trend of decreasing YOC with increasing Knudsen number. In this toy model, the shell, instead of smoothly decelerating, breaks apart and completely mixes into the fuel, quenching burn above the line in radius-time space corresponding to the maximum shell velocity (100% penetration fraction). When this model is applied, the trend of decreasing YOC with increasing N_K persists, with a yield-over-fall-line (YOF) $\sim$0.75 at $N_K \sim$0.04 (most hydrodynamic-like implosion, shot N121128) and YOF $\sim$0.12 at $N_K \sim$0.3 (most kinetic-like implosion, shot N120328).

[67] R. M. Darlington, T. L. McAbee, and G. Rodrigue, Computer Physics Communications **135**, 58 (2001).

[68] G. Dimonte and R. Tipton, Physics of Fluids **18**, 085101 (2006).

[69] O. Hurricane, D. Callahan, D. Casey, P. Celliers, C. Cerjan, E. Dewald, T. Dittrich, T. Döppner, D. Hinkel, L. B. Hopkins, J. Kline, S. Le Pape, T. Ma, A. MacPhee, J. Milovich, A. Pak, H.-S. Park, P. Patel, B. Remington, J. Salmonson, P. Springer, and R. Tommasini, Nature **506**, 343 (2014).

[70] D. T. Casey, J. A. Frenje, M. G. Johnson, M. J.-E. Manuel, H. G. Rinderknecht, N. Sinenian, F. H. Séguin, C. K. Li, R. D. Petrasso, P. B. Radha, J. A. Delettrez, V. Y. Glebov, D. D. Meyerhofer, T. C. Sangster, D. P. McNabb, P. A. Amendt, R. N. Boyd, J. R. Rygg, H. W. Herrmann, Y. H. Kim, and A. D. Bacher, Phys. Rev. Lett. **108**, 075002 (2012).

[71] C. Bellei, P. A. Amendt, S. C. Wilks, M. G. Haines, D. T. Casey, C. K. Li, R. Petrasso, and D. R. Welch, Phys. Plasmas **20**, 012701 (2013).

[72] H. G. Rinderknecht, H. Sio, J. A. Frenje, J. Magoon, A. Agliata, M. Shoup, S. Ayers, C. G. Bailey, M. Gatu Johnson, A. B. Zylstra, N. Sinenian, M. J. Rosenberg, C. K. Li, F. H. Sguin, R. D. Petrasso, J. R. Rygg, J. R. Kimbrough, A. Mackinnon, P. Bell, R. Bionta, T. Clancy, R. Zacharias, A. House, T. Dppner, H. S. Park, S. LePape, O. Landen, N. Meezan, H. Robey, V. U. Glebov, M. Hohenberger, C. Stoeckl, T. C. Sangster, C. Li, J. Parat, R. Olson, J. Kline, and J. Kilkenny, Review of Scientific Instruments **85**, 11D901 (2014).

[73] O. Larroche, Phys. Plasmas **19**, 122706 (2012).

[74]D. G. Hicks, C. K. Li, F. H. Séguin, A. K. Ram, J. A. Frenje, R. D. Petrasso, J. M. Soures, V. Y. Glebov, D. D. Meyerhofer, S. Roberts, C. Sorce, C. Stoeckl, T. C. Sangster, and T. W. Phillips, Phys. Plasmas **7**, 5106 (2000).

[75]P. Amendt, J. D. Colvin, R. E. Tipton, D. E. Hinkel, M. J. Edwards, O. L. Landen, J. D. Ramshaw, L. J. Suter, W. S. Varnum, and R. G. Watt, Phys. Plasmas **9**, 2221 (2002).